Available online at www.sciencedirect.com
ScienceDirect
Applied Catalysis B: Environmental 79 (2008) 72–80
APPLIED CATALYSIS B: ENVIRONMENTAL
www.elsevier.com/locate/apcatb

Simple fabrication of twist-like helix N,S-codoped titania photocatalyst with visible-light response

Jian-Hua Xu [a], Jingxia Li [a], Wei-Lin Dai [a,*], Yong Cao [a], Hexing Li [b], Kangnian Fan [a]

[a] Department of Chemistry and Shanghai Key Laboratory of Molecular Catalysis and Innovative Materials, Fudan University, Shanghai 200433, PR China
[b] Department of Chemistry, Shanghai Normal University, Shanghai 200234, PR China

Received 20 April 2007; received in revised form 2 October 2007; accepted 8 October 2007
Available online 13 October 2007

Abstract

Visible-light responsible N,S-codoped titania photocatalyst was fabricated by simple hydrolysis of titania tetrachloride using ammonia in the presence of glacial acetic acid and ammonium sulfate. The N,S-codoped titania materials were fabricated by a template-free route and demonstrated twist-like helix morphology. The morphology and microstructure characteristics of N,S-codoped titania photocatalysts were characterized by means of the N_2 adsorption–desorption measurements, thermal gravimetric and differential thermal analysis (TG-DTA), transmission electron microscopy (TEM), scanning electron microscopy (SEM), X-ray photoelectron spectroscopy (XPS), Fourier transform infrared spectroscopy (FT-IR), UV–visible diffuse reflectance spectra (DRS) and X-ray powder diffraction (XRD). The unique morphology of N,S-codoped titania materials and mesoporous microstructure were maintained after a heat treatment at 723 K for 3 h, exhibiting significantly thermal stability. The photocatalytic activity was evaluated by degrading phenol in aqueous suspension under ultraviolet and visible light irradiation. The results obtained with these novel photocatalysts are compared with the behavior of the well-studied and widely used Degussa P25 TiO_2 under the same conditions. The N,S-codoped titania samples were more superior than P25 and the sample calcined under 723 K for 3 h shows the best photocatalytic activity, the higher activity of which could be attributed to its high surface area, large pore volume, well-crystallized anatase, red-shift in adsorption edge and strong absorbance of light with longer wavelength.

Keywords: Titanium dioxide; Titanium tetrachloride; Mesoporous; Visible-light; N,S-codoped; Photocatalyst

1. Introduction

Semiconductor photocatalysis is an efficient method for the chemical utilization of solar energy. TiO_2, among various photocatalysts, is most frequently employed owing to its cheapness, nontoxicity, and structural stability [1–5]. However, the widespread technological use of TiO_2 is impaired by its wide band gap (ca. 3.2 eV for crystalline anatase phase) which requires the use of UV light during the reaction while the solar spectrum usually contains about 4% UV light, thus limiting the possibility of employing solar light in TiO_2 photocatalysis. Besides, the low quantum efficiency of the TiO_2 also limited its application.

Many researchers paid their much attention on anion doped photocatalysts since Sato et al. firstly reported in 1986 that nitrogen doped titanium oxide with high visible-light photocatalytic activities could be prepared by treating anatase TiO_2 powder in the NH_3 atmosphere [6–13]. Modification TiO_2 with various metal and non-metal ions were powerful ways to extend the adsorption light from UV to visible area and to reduce the recombination of photo-generated electrons and vacancies of TiO_2. N, anion-doped TiO_2 photocatalysts having an anatase form that show a relatively high level of activity when irradiated by visible light have been reported, and substitution of the lattice oxygen with nitrogen might narrow the band gap by mixing the N 1s and O 1s states. Other kind of anions such as C, S and F would result in the similar effect to nitrogen [14–19]. However, most methods are high temperature processes, using expensive precursors or preparation instruments. Besides the energy waste, the treatment at such high temperature usually resulted in the low surface area due to the undesirable sintering of nanocrystallites [12,20]. Hence, the seeking of new facile approaches to synthesize doped TiO_2 caught hold of increasingly interesting.

* Corresponding author. Tel.: +86 21 55664678; fax: +86 21 65642978.
E-mail address: wldai@fudan.edu.cn (W.-L. Dai).

0926-3373/$ – see front matter © 2007 Elsevier B.V. All rights reserved.
doi:10.1016/j.apcatb.2007.10.008

It is also known that hierarchically ordered mesoporous TiO_2 materials may be promising candidates in the field of photocatalysis owing to their large surface area and convenient mass transfer in mesopores in degrading large pollution molecules. However, these TiO_2 materials are traditionally prepared by using surfactant templating in which supramolecular aggregates are considered to direct inorganic deposition across a range of length scales [21,22]. The organic templates must then be removed by thermal treatment, resulting in high-energy consumption, environmental pollution and most important the agglomeration and collapse of pore structure in many cases [23–25]. So most reported mesoporous titania materials have a low thermal stability. To the best of our knowledge, although there were some researches related with N,S-codoped titania photocatalysts [26,27], no hierarchically ordered mesoporous N,S-codoped titania material with highly thermal stability has been reported yet by using titanium tetrachloride as the titanium precursor under mild conditions.

In the present work, we use a simple template-free approach for the synthesis of N,S-codoped titania photocatalysts with visible-light response via a low-temperature precipitation treatment of $TiCl_4$ by ammonia in the presence of glacial acetic acid and ammonium sulfate. The reaction condition is much milder than that of conventional methods. In addition, it is more interesting to find that the N,S-codoped titania sample shows a unique twist-like helix structure which has never been reported yet.

2. Experimental

2.1. Preparation of mesoporous N,S-codoped titania samples

Titanium tetrachloride ($TiCl_4$, analytical reagent grade) was used as titanium precursor. Commercially available reagents were obtained from Aldrich and used without further purification. The mesoporous N,S-codoped titania samples were prepared by hydrolysis $TiCl_4$ with ammonia in water solution in the presence of glacial acetic acid and ammonium sulfate ($(NH_4)_2SO_4$). In a typical procedure, 25 mL of dilute aqueous solution of $TiCl_4$ (3.0 mol L^{-1}) was carefully added into 150 mL deionized water with gentle stirring in ice-water bath to avoid a drastic hydrolysis of $TiCl_4$ in water at room temperature. Subsequently, 4.5 mL of glacial acetic acid and 10 g ammonium sulfate was added into the solution, then the solution was heated to 323 K. After that, a 35% (w/w) solution of ammonia was added dropwise with vigorous stirring until pH 8, then the mixed solution was quickly cooled down to ambient temperature (about 298 K) by rinsed with running water. After aging in the mother liquor for a few days, the resultant slurry was suction-filtered and washed with distilled water until pH 7 and then washed carefully with absolute ethanol for three times. The N,S-codoped titania samples were finally obtained after the as-prepared filter residue being vacuum-dried at 353 K for 12 h, followed by calcination at certain temperatures for 3 h with the rate of 10 K min^{-1}.

Six new samples, including the as-prepared precipitate and five calcined samples denoted as N,S-TiO_2-AS, N,S-TiO_2-623, N,S-TiO_2-723, N,S-TiO_2-823, N,S-TiO_2-923 and N,S-TiO_2-1023 were obtained (see Table 1).

2.2. Characterizations

XRD patterns of N,S-TiO_2 samples (2θ ranges from 20° to 70°) were recorded at room temperature with scanning speed of 2° min^{-1} using Cu Kα radiation (λ = 0.154 nm) from a 40 kV X-ray source (Bruker D8 Advance) and diffracted beam monochromator, operated at 40 mA. The Scherrer equation was applied to estimate the average crystallite sizes of TiO_2 samples: $d = 0.89\lambda/B(2\theta)\cos\theta$, where $B(2\theta)$ is the width of the XRD peak at half peak-height in radian, λ the wavelength of the X-ray in nanometer, θ the angle between the incident and diffracted beams in degree, and d is the average crystallite size of the powder sample in nanometer. The content of anatase in TiO_2 powder was calculated as follows [28]: $X_A\ (\%) = I_A/(I_A + 1.265I_R) \times 100$, where X_A is the content of the anatase phase, I_A and I_R are peak intensities of anatase (1 0 1) and rutile (1 1 0), obtained from X-ray diffraction patterns, respectively.

The textural structures were measured by N_2 adsorption at 77 K in a Micromeritics TriStar ASAP 3000 system, and specific surface areas of N,S-TiO_2 samples were measured using Brunauer–Emmett–Teller (BET) method. The pore size distributions (average pore diameter and mean pore volume) were measured from the N_2 desorption isotherm using the

Table 1
Textural and structural properties of N,S-TiO_2 samples annealed at different temperatures

Sample	Calcination temperature (K)	Surface area ($m^2\ g^{-1}$)[a]	Pore volume ($cm^3\ g^{-1}$)[a]	Average pore diameter (nm)	Crystallite phase (%)[b]	Crystallite size (nm)[c]
N,S-TiO_2-AS	R.T.	411	0.25	3.5	A-100	A-4.1
N,S-TiO_2-623	623	146	0.19	4.0	A-100	A-7.0
N,S-TiO_2-723	723	82	0.15	4.6	A-100	A-9.9
N,S-TiO_2-823	823	43	0.09	5.1	A-100	A-20
N,S-TiO_2-923	923	4	0.03	8.5	A-100	A-32
N,S-TiO_2-1023	1023	1	0.01	14.1	A-98	A-42
Degussa P25	–	51	0.16	16	A-77/R-23	A-21/R-24

[a] BET surface area, average pore volume of the N,S-TiO_2 samples estimated from nitrogen adsorption.
[b] Ratio of phase of titania based on XRD data, where A and R represent the anatase and rutile phases, respectively.
[c] Average size of titania crystallites estimated from Scherrer equation.

cylindrical pore model (BJH method). Transmission electron micrographs were obtained using a JEOL 2011 microscope operating at accelerating voltage of 200 kV. The samples for electron microscopy were prepared by dispersing the powder in ethanol and applying a drop of very dilute suspension on copper grids. The suspensions were dried by slow evaporation at ambient temperature. Scanning electron micrographs were obtained using Philips XL 30 electron microscope. The samples were deposited on a sample holder with a piece of adhesive carbon tape and were then sputtered with a thin film of gold. Simultaneous thermal gravimetric (TG) and differential thermal analysis (DTA) measurements were performed between room temperature and 1023 K on a Perkin-Elmer 7 series thermal analyzer, using Al_2O_3 as a reference. Samples were heated at a rate of 10 K min^{-1} under a dynamic dry air atmosphere of 50 mL min^{-1}. For each experiment, 10–15 mg of sample was used. X-ray photoelectron spectroscopy (XPS) measurements were performed on a PHI 5000C ESCA System with Mg Kα source at 14.0 kV and 25 mA. All the binding energies were referenced to the C 1s peak at 284.6 eV of the surface adventitious carbon. All samples were calcined under 723 K for 3 h to eliminate removable nitrogen adsorbent. The FT-IR spectra were recorded at 298 K with a Bruker Vector33 spectrophotometer using the samples of mixture of the catalyst and KBr. UV–visible diffuse reflectance spectra (UV–Vis. DRS) were achieved using a UV–visible spectrophotometer (Shimadzu UV-2450) using $BaSO_4$ as the reference sample.

2.3. Adsorption and degradation of phenol

The photocatalytic activity experiments of the N,S-TiO_2 series and Degussa P25 for the decomposition of phenol in ultraviolet and visible light irradiation were performed in a self-constructed quartz photoreactor which consists of a quartz tube (diameter 20 mm, length 250 mm) placed in the middle of the lamp bracket. Four 8 W lamps with various wavelengths (243 or 420 nm) were used as ultraviolet and visible light source. In each experiment, the catalyst of 0.050 g was placed into 50 mL of reactant solution with the initial concentration of 0.060 g L^{-1} (for ultraviolet experiment) or 0.030 g L^{-1} (for visible-light experiment) of phenol, respectively. The reaction solution was sonicated for 20 min with a sonicator to obtain a homogeneous suspension. The reactant was adsorbed on the catalyst surface without irradiation for about 60 min to achieve the adsorption/desorption equilibrium established. The temperature was controlled at 298 ± 1 K during the overall decomposition process. During all experiments, the photoreactor was continuously purged with air at a flow rate of 100 mL min^{-1} to guarantee sufficient O_2 concentration in the reaction medium. After saturation of adsorption into catalysts, 3 mL of the prepared suspension was taken as a blank probe before irradiation and, after filtration by a dialyzer with the pore of 2 μm of the catalyst, for the UV–Vis. analysis. After that, the quartz tube was put into the photoreactor and the lamps were switched on in order to start the process of decomposition. In every 0.5 h, several milliliters of solution were sampled from the reaction mixture through a membrane filter in order to measure the reactant concentration in the same way as the blank probe, while the sampling interval was 1 h for visible light photodegradation. The concentration of phenol was calculated from the height of peak at 270 nm in UV–Vis. spectra (Shimadzu, UV-2450) by using calibration curve. The measurements were repeated for each catalyst and the experimental error was found to be within ±3%. The kinetic analysis was understood in terms of modified (for solid–liquid reactions) Langmuir–Hinshewood kinetic treatment. The corresponding kinetic curve of the standard photocatalyst TiO_2 P25 (Degussa) is included for comparison purpose.

3. Results and discussion

3.1. X-ray diffraction

The crystal structure of TiO_2 depends on the temperature of heat treatment. It is commonly considered that the anatase phase of TiO_2 shows better photocatalytic activity than the rutile one. As-prepared sample without calcination as shown in Fig. 1a shows polycrystalline anatase phase. With the calcination temperature increases, the peak width and the intensity of anatase phase at $2\theta = 25.3^\circ$ become sharper and more strong, indicating the formation of larger crystallite size and higher crystallinity by increasing the calcination temperature. Because the anatase phase was present by itself, the samples would not undergo a phase transformation process from amorphous to anatase during the following moderately thermal treatment. Commonly, this kind of phase transformation is also harmful to keep high specific surface area, porosity and photoactivity [29]. Anatase-type TiO_2 could be obtained from not only the as-prepared sample but also those samples even heated up to 1023 K for 3 h, during which little rutilization existed, indicate the N,S-codoped TiO_2 samples exhibit considerably high thermal stability and highly resistant to

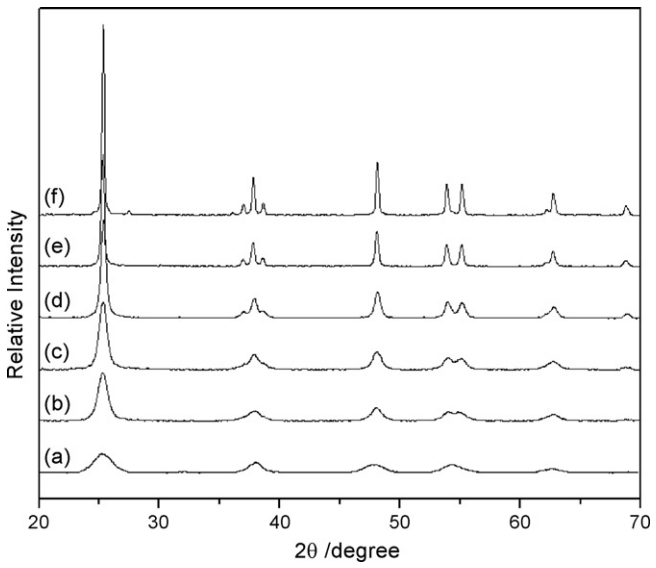

Fig. 1. X-ray diffraction patterns of N,S-codoped titania samples. (a) N,S-TiO_2-AS; (b) N,S-TiO_2-623; (c) N,S-TiO_2-723; (d) N,S-TiO_2-823; (e) N,S-TiO_2-923 and (f) N,S-TiO_2-1023.

the phase transformation to rutile. The characteristic parts of XRD patterns of the as-prepared anatase TiO_2 and the samples calcined at 623, 723, 823, 923, and 1023 K are shown in Table 1. Powder XRD was used for crystal phase identification and the crystallite size of each phase present. The anatase (1 0 1) peak at $2\theta = 25.3^\circ$ and the rutile (1 1 0) peak at $2\theta = 27.6^\circ$ were analyzed using the formula in order to estimate the anatase–rutile ratio of TiO_2 samples: $X_R = (1 + 0.8I_A/I_R)^{-1}$, where X_R is the weight fraction of rutile in the powders, and I_A and I_R are the XRD peak intensities of the anatase and rutile phases, respectively.

The XRD pattern of the powder heated at 1023 K shows the anatase (1 0 1) and the emerging peak of rutile (1 1 0), indicating that the sample N,S-TiO_2-1023 (Fig. 1f) is a mixture of anatase and rutile. The N,S-TiO_2-1023 sample contains 98% of anatase and 2% of rutile and exhibits sharp XRD lines with a few signs of broadening. The average size of crystallites was calculated from the peak half-width B, using the Scherrer equation [30], $d = k\lambda/B(2\theta)\cos\theta$, where k is a shape factor of the particle (it equals to 1 if a spherical shape is assumed), λ and θ the wavelength and the incident angle of the X-rays, and B the full width half maximum (FWHM) of the 2θ peak, respectively. The peak width was measured at half of the maximum intensity. The estimation shows that the mean crystallite size of the initial anatase TiO_2 individual particles (N,S-TiO_2-AS) was about 4.1 nm, supposing that the broadening of peak is due to the size effect. Calcination is usually accompanied with crystal growth [31], the crystallite size of each sample is presented in Table 1.

3.2. Particle morphology

Fig. 2a–e shows the SEM micrographs of the N,S-TiO_2-623, N,S-TiO_2-723, N,S-TiO_2-823, N,S-TiO_2-923 and N,S-TiO_2-1023 for each sample dried or annealed for 3 h at corresponding temperatures. The SEM images of the N,S-TiO_2 anatase samples revealed that the titania powder demonstrated twist-like helix morphology and could be preserved well after calcination. The average screw-pitch of each twist is about 10 μm, the array of ventages exhibited regularly between conterminous twists, and the average diameter of each hole is about 2 μm × 5 μm with the interval of ca. 4 μm. An expanded view in inset (a) gives a brief sight of N,S-TiO_2-623. The size of twist-like TiO_2 sample was comparatively uniformly sized. The shape of these samples remains almost unchanged after the thermal treatment process even the N,S-TiO_2 samples are calcined at 823 K for 3 h, only a little distortion was observed. With the calcination temperature increases, the twist-like TiO_2 sample becomes shrinking and significantly sintered after calcined under 923 and 1023 K, respectively (Fig. 2d and e), while the samples were shattered and tremendously shrunk to irregular curves.

TEM analyses were performed to examine the nanocrystallites that make up the twist-like helix N,S-TiO_2 samples. Fig. 2f presents the nanocrystalline nature of anatase TiO_2. It is found that the size of anatase nanocrystallites is approximately 4–5 nm, which is consistent well with that calculated from the XRD data (see Table 1). High resolution TEM confirmed that the sample were comprised of connected crystalline titania nanoparticles with a lattice spacing consistent with the anatase phase (0.352 nm), giving evidence the polycrystalline nature for N,S-TiO_2-AS sample which fit well with the XRD patterns. Such anatase crystallinity in the mesoporous TiO_2 is highly desirable in photocatalysis [32]. The electron diffraction measurement of the selected area (Fig. 2f, inset) demonstrated clear diffraction lines representative of anatase, namely, (1 0 1), (2 0 0), (0 0 4) and (2 1 1), further indicating that the sample was in well-crystallized anatase phase and it was also confirmed by the result of X-ray diffraction.

The formation of hierarchical porous shapes was usually explained by facet selectivity of the templates during the crystallite growth of the synthesis. While no template is used in our present work for the synthesis, the formation of twist-like helix morphology happens during the processing. There might be another mechanism for the formation of TiO_2 microtubes, we find the use of acetic acid as a dispersing agent is of crucial importance in the preparation of apertured titania microtube structure. The essential role of acetic acid in promoting the formation of mesoporous TiO_2 microtubes may be understood by taking into account the behaviour as a ligand and the modification of the polymeric structure at a molecular level, which promoted the emergence of polymeric structures [33]. An elucidation of such a mechanism is beyond the scope of the present work.

3.3. The specific surface area, pore size and pore volume

The specific surface area of the samples is measured using the BET method by N_2 adsorption and desorption at 77 K. Table 1 shows the physicochemical properties of N,S-TiO_2 series dried or calcined at temperatures ranging from ambient temperature to 1023 K. The as-prepared sample (i.e. N,S-TiO_2-AS) showed a specific surface area of 411 $m^2\ g^{-1}$, about eight times larger than Degussa P25, also much higher than the reported TiO_2 obtained by conventional method [34,35]. While the sample was calcined at 723 or 823 K for 3 h, it still presented a comparatively high specific surface area of 82 or 43 $m^2\ g^{-1}$, respectively. In this range of thermal treatment temperature, the titania samples shows best photoactivity in the decomposition of aqueous phenol solution, significantly higher than P25. Although there is still much debating on whether activity of a photocatalyst can be related to the catalyst surface area, since photocatalytic reactions are believed to proceed only on the illuminated surface. However, one could argue that adsorption on the catalyst surface would at least help to ‘‘concentrate’’ the reactant molecules for the photoreactions and the photos might be scattered between the nano-sized TiO_2 particles. Also, photogenerated electrons and vacancies as well as the adsorbed molecules might be able to diffuse more or less at the catalyst surface, causing the photoreactions more easy to happen [36]. The high specific surface area of N,S-TiO_2 sample may help this process more efficiently in photodegradation. With a higher calcination temperature, the surface area of the samples were seen to reduce to 4 $m^2\ g^{-1}$ (N,S-TiO_2-923) and 1 $m^2\ g^{-1}$ (N,S-TiO_2-1023) when the calcination temperature

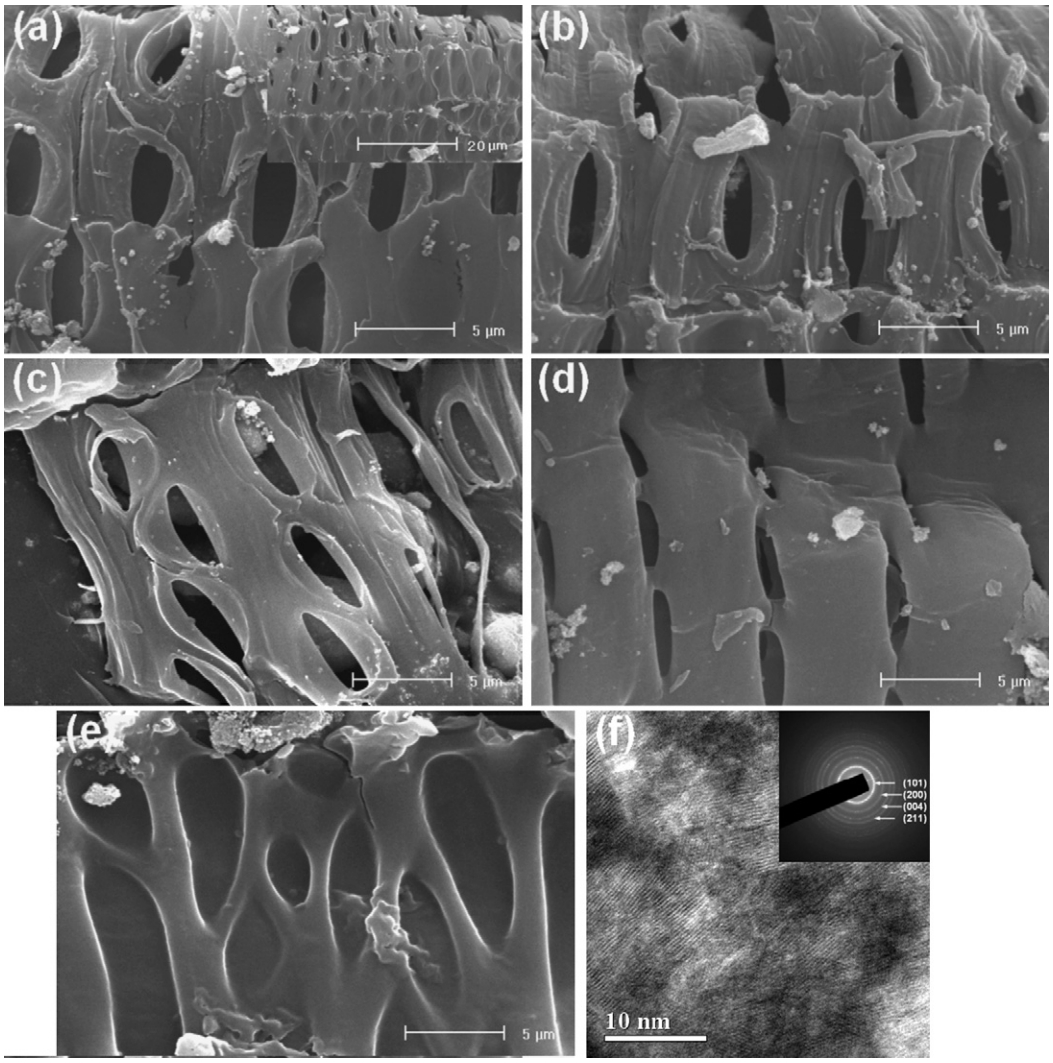

Fig. 2. SEM images of N,S-TiO_2 samples. (a) N,S-TiO_2-623; (b) N,S-TiO_2-723; (c) N,S-TiO_2-823; (d) N,S-TiO_2-923; (e) N,S-TiO_2-1023 and TEM images of N,S-TiO_2-AS (f). The SAED image in inset (f) displaying the crystalline nature (anatase) of the titania nanoparticles.

was further increased to 923 and 1023 K, respectively. The variation of the sample pore volume, with the calcinations temperature, followed the same trend of the surface area. The average pore volume of N,S-TiO_2-AS sample was 0.25 $cm^3\ g^{-1}$. With the increase of calcination temperature, the pore volume becomes smaller, accompanied with the decrease of photoactivity.

Fig. 3 shows the nitrogen adsorption–desorption isotherm of the as-synthesized N,S-TiO_2 sample, which indicates a type IV-like isotherm with an inflection of nitrogen-adsorbed volume at $P/P_0 = 0.45$ (type H_2 hysteresis loop), indicating the presence of well-developed mesoporosity in the twist-like helix N,S-codoped titania samples. Moreover, the inset in Fig. 3 shows the pore-size distribution plots calculated using the Barrett–Joyner–Halenda (BJH) equation from the adsorption branch of the isotherm. The pore size distribution measurement indicates that the twist-like helix N,S-codoped titania sample has pronounced mesoporosity of a narrow pore-size distribution with an average pore diameter at ca. 3.5 nm. These results illustrate that the doping with N or S species does not

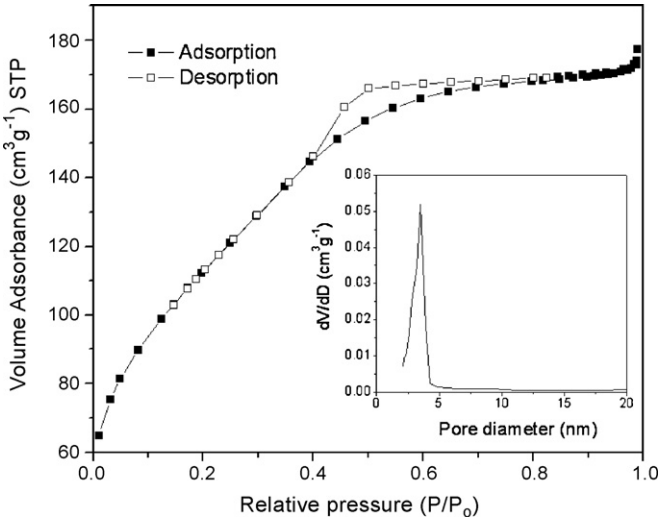

Fig. 3. Nitrogen adsorption/desorption isotherms and the corresponding pore size distribution (inset) of N,S-TiO_2-AS.

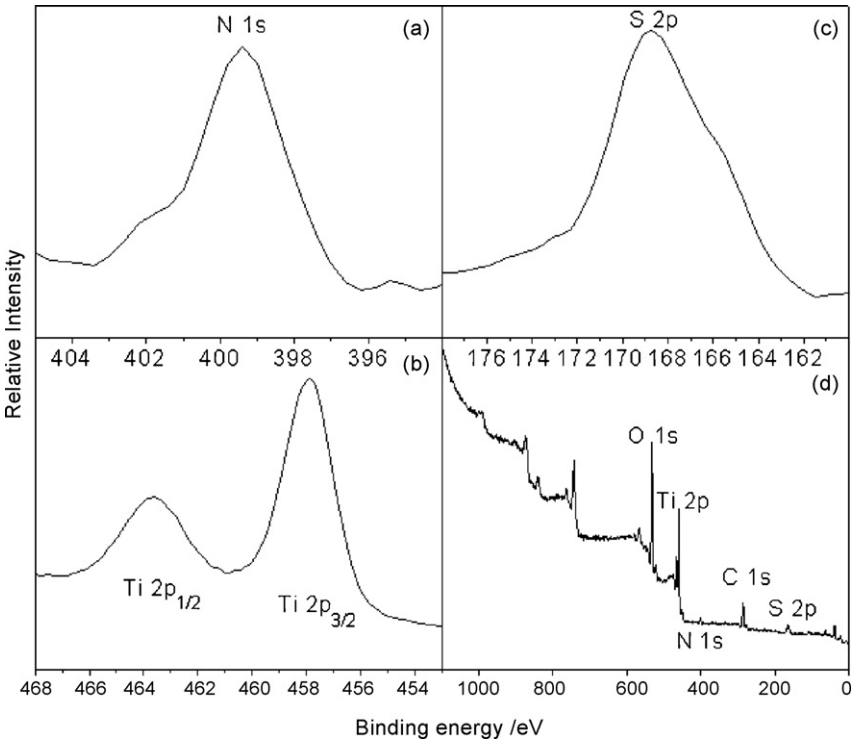

Fig. 4. (a) XPS spectra of the N 1s; (b) S 2p; (c) Ti 2p and (d) full regions for the N,S-TiO_2-723 sample.

significantly change the textural properties of TiO_2. The dopants are embedded in the TiO_2 network or chemisorbed on the surface of the mesoporous pore walls, and the pore channels remain open. Such open mesoporous architecture, large surface area and 3D-connected pore system, play an important role in catalyst design for its ability to improve the molecular transport of reactants and products [37]. The mesoporous structure was maintained after 733 K calcination, but the pore volume was lessened and the average pore size was gently increased. It is known that commercial Degussa P25 shows no mesoporosity, which might be one reason why the present N,S-TiO_2 sample shows much higher photoactivity than that of P25.

3.4. XPS and FT-IR analysis

The well crystallization and high stablility of N,S-TiO_2 photocatalyst can be explained by the XPS spectra (Fig. 4). The nitrogen and sulfur elements could be chemically adsorbed on the TiO_2 surface or doped into TiO_2 lattice, and the adsorbed elements could be eliminated by thermal treatment. The characterization was performed after calcined at 723 K for 3 h in order to eliminate the physically adsorbed N or S species and the results confirmed the existence of doping or strong chemical adsorption of them.

XPS survey spectrum showed that after calcination, the nitrogen and sulfur percentage in the N,S-TiO_2 remain 2.0% and 2.9%, respectively. A small amount of carbon element was ascribed to the adventitious hydrocarbons from the XPS instrument itself. Two kinds of N species were detected in the N 1s region. Most N species existed in the nitrides, corresponding to the binding energy of 399.5 eV, while only trace N species were present in the form of surface adsorbed NH_3 molecules, with the binding energy located at 395.4 eV [38], which can prove the formation of N–Ti–O bond [20,39]. The formation of these bonds can inhibit the aggregation of titania particles and enhance the crystallization degree of anatase phase during calcination process. Meanwhile, the peak of S 2p around 168.5 eV shifted negatively by 0.5 eV in comparison with the standard binding energy of the sulfur in pure SO_4^{2-} (169.0 eV), which was also proved by other groups [40]. These results demonstrated that electrons partially transferred from oxygen to sulfur in N,S-TiO_2 because of the existence of Ti^{4+}. The possible coordination models between SO_4^{2-} and TiO_2 can be understood from Scheme 1. The difference of the S 2p binding energy indicated the presence of the Ti–O–S bond which resulted in the change of the chemical circumstance of sulfur, so that the SO_4^{2-} could coordinate with TiO_2 in the network which could increase the activity from following points.

As it has been previously reported, pre-treatment with sulfate of TiO_2-precursor and further calcination produces interesting stabilization surface area and anatase phase at rather high temperature. It is well-established that doped sulfur atoms retain the anatase structure avoiding rutilization process, which is stated to be a topotactic transformation. Information given by

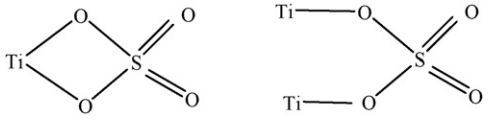

Scheme 1. Coordination models between SO_4^{2-} and TiO_2.

XRD and Raman spectroscopy supports this statement [41,42]. On the other hand, in addition to the structural stabilization during calcination, acidification of TiO_2-precursor with sulfuric acid produces an increase of the adsorbed protons. The excess of surface protons in the precursor affects the OH^-/H^+ equilibrium on the surface. According to the above XPS results, it can be inferred that N and S elements were in situ codoped into TiO_2 during hydrolysis of $TiCl_4$ with ammonia, and the N and S elements came from ammonium sulfate and ammonia, respectively.

To give additional evidence and further to confirm the doping of sulfur, FT-IR characterizations were performed. The infrared spectroscopy of N,S-TiO_2 and P25 are represented in Fig. 5. The absorption peak present on the spectra of N,S-TiO_2 at 1404 cm^{-1} was attributed to the adsorption of SO_4^{2-} with bidentate bond. It was reported that the absorption band near 1400 cm^{-1} results in the super acidity of catalysts [43]. After thermal treatment, the peak intensity weakened along with the elimination of physical adsorbed SO_4^{2-}, chemisorbed and doped SO_4^{2-} species were remaining existence, however, the above absorption peak do not exist in the P25 catalyst. This result is in well accordance with the XPS results, since the binding energy of S element shift negatively to form the Ti–O–S bonds. However, the doping character of sulfur element may not be similar to that of the nitrogen, considering the SO_4^{2-} with bidentate bond cannot easily replace the Ti^{4+} ion and enter the internal TiO_2 lattice. The most possible doping process is that the SO_4^{2-} chemisorbed on the surface of the catalyst, edges and the lattice holes to form strong interaction during higher temperature treatment process, which may produce Ti–O–S bonds as proved by XPS. Since SO_4^{2-} doped TiO_2 exhibits a higher acidity than pure TiO_2, doping with SO_4^{2-} can modify the affinity of substrates for the catalyst surface, and as a consequence, the adsorption equilibrium and photoxidation activity of the catalysts.

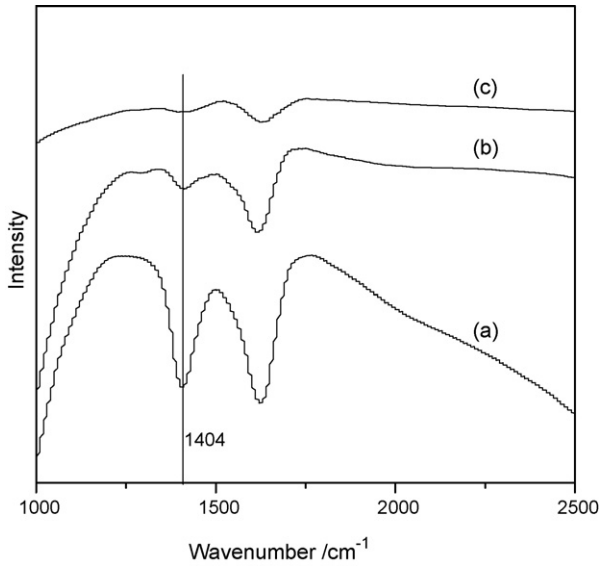

Fig. 5. FT-IR spectra of samples: (a) N,S-TiO_2-AS; (b) N,S-TiO_2-723 and (c) Degussa P25.

3.5. UV–Vis. diffuse reflectance spectra

The UV–Vis. diffuse reflectance spectra (DRS) of the mesoporous N,S-TiO_2 samples are shown in Fig. 6. N and S codoping expand the wavelength response range of TiO_2 into the visible region and the optical band edge of the mesoporous N,S-TiO_2 exhibits a remarkable red-shift with respect to that of pure TiO_2 (P25). The absorbance increases with the rise of calcination temperature, this may be attributed to the fact that the high-temperature calcination can induce N and S elements doped into the lattice of TiO_2, resulting in the enhancive red shift [26]. The red shift is ascribed to the fact that N,S-codoping can narrow the bad gap of the TiO_2, and the direct band gap energy of N,S-codoped TiO_2 powders was decreased, smaller than crystalline anatase phase TiO_2 (ca. 3.2 eV) and P25 (ca. 3.1 eV). This result further approved the substitution of crystal lattice O or Ti to dopant species, which is consistent with the XPS results. The enhanced ability to absorb visible light makes this mesoporous N,S-TiO_2 an effective photocatalyst for solar-driven applications.

3.6. Photocatalytic activity of TiO_2 samples in photodegradation of phenol

To evaluate and compare the photocatalytic activity of the mesoporous N,S-TiO_2 samples, the reactions of phenol degradation were performed as photoreaction probes under UV and visible irradiation. The course of phenol photodecomposition using the catalyst N,S-TiO_2 series annealed at various temperatures are given in Fig. 7. Degussa P25 was used as the reference material for comparison purpose. In the controlled experiment in which phenol is in TiO_2 suspensions in the dark or is illuminated with ultraviolet light in the absence of TiO_2 does not exhibit photocatalytic activity.

Most of the samples demonstrate considerably high photoactivity under ultraviolet irradiation (Fig. 7a). It was

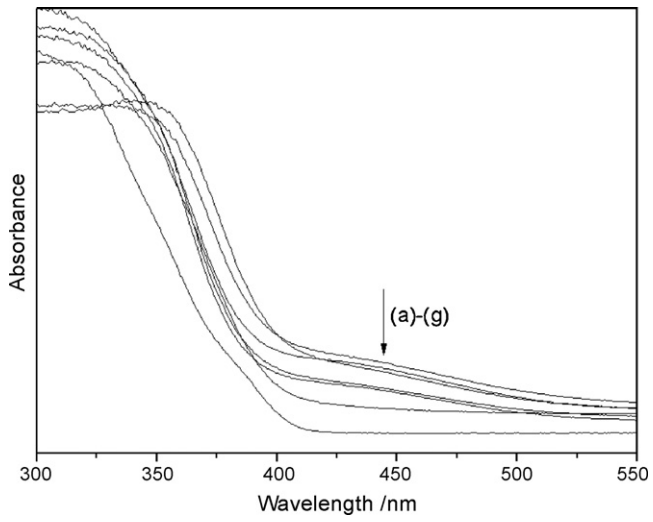

Fig. 6. UV–visible diffuse reflectance spectra of (a) N,S-TiO_2-923; (b) N,S-TiO_2-823; (c) N,S-TiO_2-1023; (d) N,S-TiO_2-723; (e) N,S-TiO_2-623; (f) N,S-TiO_2-AS and (g) Degussa P25.

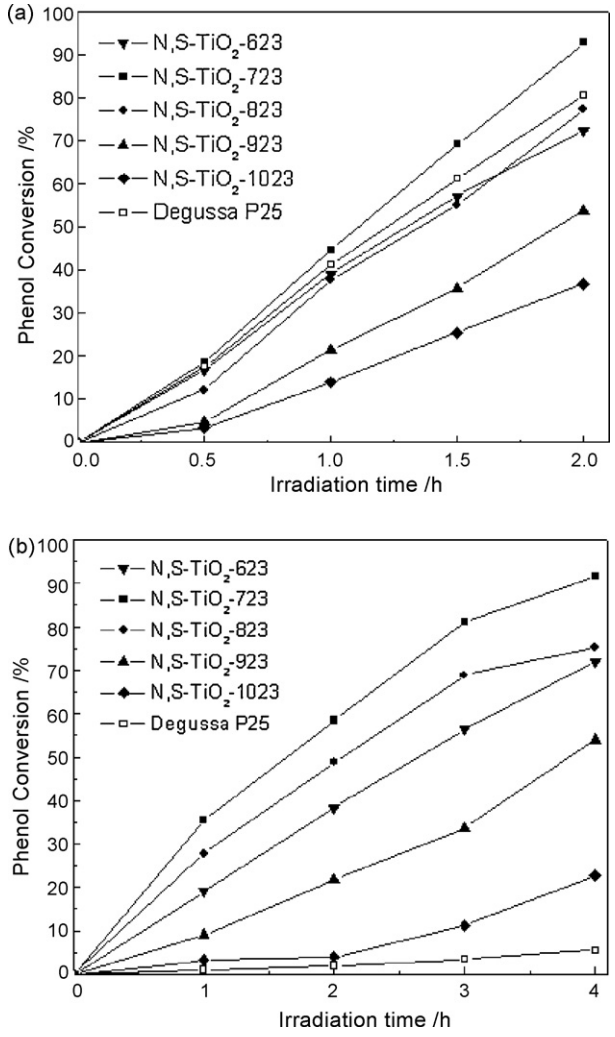

Fig. 7. Time courses of the photocatalytic decomposition of phenol on annealed N,S-TiO_2 samples and Degussa P25. (a) Under ultraviolet irradiation; (b) under visible irradiation.

found that the N,S-TiO_2-723 sample exhibited the best photocatalytic efficiency on the degradation of phenol of all the tested TiO_2 samples and phenol was almost completely eliminated within 2 h. It is evident that the photoactivity of the sample calcined at proper temperature is superior to the standard photocatalyst Degussa P25. The high photocatalytic activity of the N,S-TiO_2-723 sample is partially due to its high specific surface area, small crystallite size and good anatase crystallization. After annealing at temperatures of 823 K the activity decreased while at a even higher calcination temperature, the photocatalytic activity of N,S-TiO_2-1023 decreased significantly, with the nanocrystallite sintering and growth, significant decrease of surface area and the starting of the phase transformation from anatase to rutile.

In the visible light region (420 nm, see Fig. 7b), the N,S-TiO_2-723 photocatalyst keep relativity high performance while P25 has nearly no activity at all. The expanded photoactivity under visible light is due to the nitrogen and sulfur doping according to the commonly accepted opinions and the interface between the two phases of undoped TiO_2 and N,S-codoped TiO_2 may act as a rapid separation site for the photo-generated electrons and holes due to the difference in the energy level of their conduction bands and valence bands. The red shift in the band gap transition of the N,S-codoped TiO_2 samples indicated that more photo-generated electrons and vacancies can participate in the photocatalytic reactions. The excellent photocatalytic activity of the N,S-TiO_2-723 sample could also be attributed to the well-crystalline anatase phase which facilitates the transfer of photo-induced vacancies from bulk to surface for degradation of organic compounds and effectively inhibits the recombination between the photo-induced vacancies and electrons which may enhance the quantum yield [40]. The photocatalytic performance is also related to the mesoporous microstructure of the N,S-TiO_2 samples with large BET surface areas and a 3D-connected pore system which can help to concentrate the reactant molecules for the photoreactions and the photos might be scattered between the nanosized TiO_2 particles [36].

4. Conclusions

In summary, we have demonstrated a facile and template-free method for the fabrications of visible-light responsible N,S-codoped titania photocatalyst with remarkable thermal stability and extremely high specific surface area. The N,S-TiO_2 samples were synthesized by simple hydrolysis of titania tetrachloride using ammonia in the presence of glacial acetic acid and ammonium sulfate. The novel photocatalysts show high visible-light photocatalytic activity in degrading phenol while the N,S-TiO_2-723 sample gives the best photocatalytic activity and demonstrates to be far superior to that of the commercial Degussa P25 counterpart. The doped nitrogen and sulfur species play a key role in expanding the photoactivity to visible light region, narrowing the band gap, and improving the anatase crystallization and thermal stability. The high photoactivity of the N,S-codoped TiO_2 can be attributed to the results of the synergetic effects of its high surface area, large pore volume, well-crystallized anatase, red shift in adsorption edge and strong absorbance of light with longer wavelength. Further work for the examination of the formation mechanism of these twist-like helix samples is being under way.

Acknowledgements

We are grateful to the financial supports from the Major State Basic Resource Development Program (Grant no. 2003CB615807), NSFC (Project 20573024, 20407006), and the Natural Science Foundation of Shanghai Science & Technology Committee (06JC14004).

References

[1] A.L. Linsebigler, G.Q. Lu, J.T. Yates, Chem. Rev. 95 (1995) 735.
[2] A. Fujishima, T.N. Rao, D.A. Tryk, J. Photochem. Photobiol. C 1 (2000) 1.
[3] C. Kormann, D.W. Bahnemann, M.R. Hoffmann, J. Phys. Chem. 92 (1988) 5196.
[4] S. Klosek, D. Raftery, J. Phys. Chem. B 105 (2001) 2815.
[5] S. Quadawi, S.R. Salman, J. Photochem. Photobiol. A 48 (2002) 161.

[6] S. Sato, Chem. Phys. Lett. 123 (1986) 126.
[7] R. Asahi, T. Morikawa, T. Ohwaki, K. Aoki, Y. Taga, Science 293 (2001) 269.
[8] J. Ovenstone, J. Mater. Sci. 36 (2001) 1325.
[9] J. Moon, H. Takagi, Y. Fujishiro, M. Awano, J. Mater. Sci. 36 (2001) 949.
[10] J.C. Yu, J.G. Yu, W.K. Ho, Z.T. Jiang, L.Z. Zhang, Chem. Mater. 14 (2002) 3808.
[11] Z.H. Yuan, J.H. Jia, L.D. Zhang, Mater. Chem. Phys. 73 (2002) 323.
[12] H. Irie, Y. Watanabe, K. Hashimoto, J. Phys. Chem. B 107 (2003) 5483.
[13] J.S. Park, W. Choi, Langmuir 20 (2004) 11523.
[14] Y. Sakatani, K. Okusato, H. Koike, H. Ando, Photocatalysis 4 (2001) 51.
[15] T. Ihara, M. Ando, S. Sugihara, Photocatalysis 5 (2001) 19.
[16] T. Umebayashi, T. Yamaki, H. Ito, K. Asai, Appl. Phys. Lett. 81 (2002) 454.
[17] H. Irie, Y. Watanabe, K. Hashimoto, Chem. Lett. 32 (2003) 772.
[18] S. Sakthivel, H. Kisch, Angew. Chem. Int. Ed. 42 (2003) 4908.
[19] W. Ho, J.C. Yu, S.C. Lee, Chem. Commun. 10 (2006) 1115.
[20] C. Burda, Y.B. Lou, X.B. Chen, A.C.S. Samia, J. Stout, J.L. Gole, Nano Lett. 3 (2003) 1049.
[21] A. Leonard, J.L. Blin, B.L. Su, Chem. Commun. 20 (2003) 2568.
[22] W.H. Deng, M.W. Toepke, B.H. Shanks, Adv. Funct. Mater. 13 (2003) 61.
[23] C.C. Wang, J.Y. Ying, Chem. Mater. 11 (1999) 3113.
[24] C. Su, B.Y. Hong, C.M. Tseng, Catal. Today 96 (2004) 119.
[25] K. Hashimoto, K. Wasada, N. Toukai, H. Kominami, Y. Kera, J. Photochem. Photobiol. A 136 (2000) 103.
[26] J.G. Yu, M.H. Zhou, B. Cheng, X.J. Zhao, J. Mol. Catal. A 246 (2006) 176.
[27] S. Yin, K. Ihara, Y. Aita, M. Komatsu, T. Sato, J. Photochem. Photobiol. A 179 (2006) 105.
[28] R.A. Spurr, H. Myers, Anal. Chem. 29 (1957) 760.
[29] D. Grosso, G. Soler-Illia, E.L. Crepaldi, F. Cagnol, C. Sinturel, A. Bourgeois, A. Brunet-Bruneau, H. Amenitsch, P.A. Albouy, C. Sanchez, Chem. Mater. 15 (2003) 4562.
[30] F.J. Pocock, J.F. Stewart, J. Eng. Power Trans. ASME 85 (1963) 33.
[31] G.V. Vasilenko, V.I. Zarembo, A.A. Slobodov, Russ. J. Appl. Chem. 70 (1997) 1498.
[32] M.R. Hoffmann, S.T. Martin, W.Y. Choi, D.W. Bahnemann, Chem. Rev. 95 (1995) 69.
[33] M.T. Tsai, J. Non-Cryst. Solids 298 (2002) 116.
[34] T. Kasuga, M. Hiramatsu, A. Hoson, T. Sekino, K. Niihara, Adv. Mater. 11 (1999) 1307.
[35] G.Q. Guo, J.K. Whitesell, M.A. Fox, J. Phys. Chem. B 109 (2005) 18781.
[36] H. Wang, Y. Wu, B.Q. Xu, Appl. Catal. B: Environ. 59 (2005) 139.
[37] J.C. Yu, G.S. Li, X.C. Wang, X.L. Hu, C.W. Leung, Z.D. Zhang, Chem. Commun. 25 (2006) 2717.
[38] H.X. Li, J.X. Li, Y.I. Huo, J. Phys. Chem. B 110 (2006) 1559.
[39] J.L. Gole, J.D. Stout, C. Burda, Y.B. Lou, X.B. Chen, J. Phys. Chem. B 108 (2004) 1230.
[40] H.X. Li, G.S. Li, J. Zhu, Y. Wan, J. Mol. Catal. A: Chem. 226 (2005) 93.
[41] G. Colon, M.C. Hidalgo, J.A. Navio, Appl. Catal. B: Environ. 45 (2003) 39.
[42] G. Colon, M.C. Hidalgo, G. Munuera, I. Ferino, M.G. Cutrufello, J.A. Navio, Appl. Catal. B: Environ. 63 (2006) 45.
[43] C. Liao, W. Hua, J. Chen, Z. Gao, Sci. China (Ser. B) 26 (1996) 275.